

Kari Kuivalainen

# Testing of the On-board Computer for Mars Meteorological Network Station

---

Helsinki Metropolia University of Applied Sciences

Bachelor of Engineering

Information Technology

Thesis

8 February 2017

Tekijä(t)	Kari Kuivalainen
Otsikko	Marsin meteorologisen verkkoaseman ohjaustietokoneen testaaminen
Sivumäärä	30 sivua + 1 liite
Aika	8.2.2017
Tutkinto	Insinööri (AMK)
Koulutusohjelma	Tietotekniikka
Suuntautumisvaihtoehto	Sulautetut järjestelmät
Ohjaaja(t)	Lehtori Anssi Ikonen Tutkija Taavi Rouhiainen Esimies Ari-Matti Harri
<p>Insinööriyön tarkoituksena oli testata muutamia MetNet-laskeutujan ohjaustietokoneen testimallin toimintoja. MetNet on Ilmatieteen laitoksen vetämä ja rahoittama monikansallinen projekti, jonka tarkoitus on valmistaa Marsin pinnalle lähetettävä laskeutuja. Useat yhdessä toimivat MetNet-laskeutujat muodostaisivat laaja-alaisen sääasemaverkon. Samanaikaisesti monesta pisteestä suoritettavat mittaukset antavat laajemman ymmärryksen Marsin ilmakehän käyttäytymisestä.</p> <p>Insinööriyössä testattu laite on ohjaustietokoneen testimalli, joka on testaamisen helpottamiseksi rakennettu väljemmin. Testimallin piirilevy on rakennettu käyttäen tavallisia komponentteja avaruuskelpoisten komponenttien sijaan. Insinööriyössä suoritettiin useita testejä tietokoneen eri piireille. Testejä varten rakennettiin ensin testausympäristö, jonka avulla tietokoneen eri toimintoja pystyi ohjaamaan.</p> <p>Testausympäristön rakentamiseen käytettiin Freescale CodeWarrior -ohjelmistokehitysympäristöä, joka sisältää ohjelmointi- ja virheenjäljitintyökalut tietokoneessa käytetyille mikrokontrollerille. Testimittauksiin ja virheiden etsimiseen käytettiin useita työkaluja, kuten oskilloskooppia ja yleismittaria.</p> <p>Insinööriyön lopputuloksena tietokoneen suunnitelmaan esitettiin muutoksia. Joistakin piireistä löydettiin puutteita. Näiden tulosten perusteella uuden insinöörimallin rakentaminen voi alkaa.</p>	
Avainsanat	Mars, MetNet laskeutuja, Testaaminen, Elektroniikka

Author(s)	Kari Kuivalainen
Title	Testing of the on-board computer for Mars meteorological network station
Number of Pages	30 pages + 1 appendix
Date	8 February 2017
Degree	Bachelor of Engineering
Degree Programme	Information Technology
Specialisation option	Embedded Design
Instructor(s)	Anssi Ikonen, Senior Lecturer Taavi Rouhiainen, Researcher Ari-Matti Harri, Supervisor
<p>The aim of this thesis was to test some of the functionalities of the MetNet Lander (MLN) lander's On-Board Computer (OBC) test model. The Meteorological Network (MetNet) mission, led and funded by the Finnish Meteorological Institute (FMI), is a multinational project with the goal of developing a spacecraft system that could operate on the surface of Mars. Several of these landers are to form a distributed weather network, providing simultaneous global measurements that could increase the understanding of Martian climate.</p> <p>The Test Model (TM), a modified version of the on-board computer, was built to make testing easier. Common-Off-The-Shelf (COTS) parts are used in place of space certified components, and the components are sparsely distributed on the breadboard. Measurements and tests were conducted on various circuits on the computer. A test software suite for operating the computer's interfaces was built. An integrated development environment was used for programming the microcontrollers and debugging the test software. Electronics laboratory equipment, such as multimeters and oscilloscope, was used for solving problems and conducting test measurements.</p> <p>As a result of this thesis, a list of changes to the OBC are proposed. Some circuits were found to be lacking. With the results from these tests, the development of a new engineering model can begin.</p>	
Keywords	Mars, MetNet lander, Testing, Electronics

## Contents

1	Introduction	1
2	Background	2
2.1	Research of Mars	2
2.2	FMI's role in Mars research	3
2.3	MetNet mission overview	3
3	MetNet on-board computer	5
3.1	General design information	5
3.2	Peripherals & interfaces	6
3.3	Development process	7
4	Test environment and process	8
4.1	Test hardware and equipment	8
4.2	Development of test software	10
5	Test plan and procedure	12
5.1	Reset switch	12
5.2	Battery charging	13
5.3	Sensor power interfaces	16
5.4	Pyrotechnics	16
5.5	CAN bus	17
5.6	RS422 interface	18
5.7	External memory	19
6	Test results	22
6.1	Reset switch	22
6.2	Battery charging	22
6.3	Sensor power interfaces	23
6.4	Pyrotechnics	25
6.5	CAN bus	26
6.6	RS422 interface	26
6.7	External memory	26
7	Conclusion	28

Appendices

Appendix 1 List of proposed changes

## Abbreviations

<b>CAN</b>	Controller Area Network
<b>COTS</b>	Common-Off-The-Shelf
<b>EDL</b>	Entry-Descent-Landing
<b>EM</b>	Engineering Model
<b>ESA</b>	European Space Agency
<b>FM</b>	Flight Model
<b>FMI</b>	Finnish Meteorological Institute
<b>GPIO</b>	General Purpose Input Output
<b>IBU</b>	Inflatable Breaking Unit
<b>IDE</b>	Integrated Development Environment
<b>INTA</b>	Instituto Nacional de Técnica Aeroespacial
<b>LED</b>	Light Emitting Diode
<b>Li-ion</b>	Lithium Ion
<b>LVDS</b>	Low-Voltage Differential Signaling
<b>MCU</b>	Microcontroller Unit
<b>MetNet</b>	Meteorological Network
<b>MLN</b>	MetNet Lander
<b>NASA</b>	National Aeronautics and Space Administration
<b>NTC</b>	Negative Temperature Coefficient
<b>OBC</b>	On-Board Computer
<b>PCB</b>	Printed Circuit Board
<b>PSU</b>	Power Supply Unit
<b>REMS</b>	Rover Environmental Monitoring station
<b>RX</b>	Receive
<b>SCI</b>	Serial Communications Interface
<b>SPI</b>	Serial Peripheral Interface
<b>TM</b>	Test Model
<b>TX</b>	Transmit
<b>USB</b>	Universal Serial Bus

## 1 Introduction

This thesis documents the process of testing the functionality of some of the electronics of the MetNet lander on-board computer test model. The MLN is part of the Mars MetNet mission, a multinational project led by FMI, which aims to establish a network of weather stations on the surface of Mars.

The Finnish Meteorological institute has been working on the MetNet mission since the early 2000s. A new version of the MetNet lander's on-board computer was built in-house at FMI and completed by the end of 2015. In order to continue the development of the computer, the design had to be tested to see whether it functioned up to specifications.

With the help of the Printed Circuit Board (PCB) schematic, a list was made detailing each interface to be tested. After the plans were formed, focus was diverted to creating the test software. Some problems were encountered while building the test software, and later during the actual testing process. Some of these problems and the process of solving them are documented in more detail.

There were a few shortcomings and potential problems in the design that were identified during testing. Some circuits and implementations were revised based on the findings of these tests. The next step is building an improved Engineering Model (EM) to proper dimensions and component placement layout.

Some of the modifications presented here and the initial work on the testing were conducted by Mr. Rouhiainen, a researcher at FMI, who is also responsible for the current design of the OBC. The thesis was done for the Radar & Space Technology Group of FMI.

## 2 Background

### 2.1 Research of Mars

Mars has been the object of scientific curiosity ever since the first observations by ancient Egyptian astronomers were made. Yet it was not until the 17th century that Mars was finally directly observed when Galileo Galilei became the first person to see Mars through a telescope. The research on Mars has taken huge strides forward in just a few centuries after Galilei, culminating in frequent robotic missions being sent to the planet since the latter half of the 20th century. [1.]

Mars research really gained momentum in the 1960s during the cold war, when the United States of America and the Soviet Union were eager to demonstrate their technological prowess. Numerous failed attempts to land on the red planet followed, with both countries dispatching multiple probes and landers in the decades after. [1.]

The American made Mariner 4 probe achieved the first successful flyby of Mars in 1965, returning 21 images to Earth [2]. The Soviets, in turn, attained the first soft landing on the planet only six years later with the Mars 3 probe touching down in 1971, albeit losing transmission some 15 seconds later. The Mars 3 orbiter, on the other hand, was more successful in its mission, delivering images and scientific measurements. [3.]

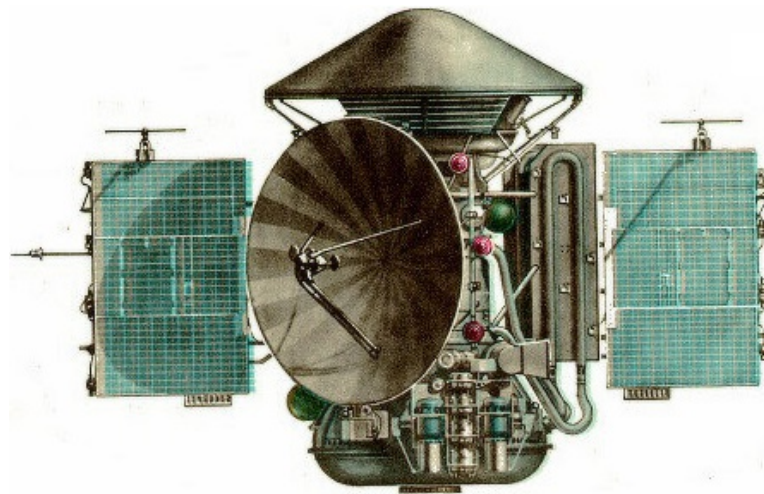


Figure 1: Mars 3 orbiter with the lander mounted on top. Copied from [www.iki.rssi.ru](http://www.iki.rssi.ru) [4].



The Viking missions by National Aeronautics and Space Administration (NASA) in 1976 were the first landers to successfully operate on Martian surface. The Viking 1 lander carried with it a biological laboratory and a weather instrument package. The landers made atmospheric observations measuring temperature and pressure. It was revealed through these findings that Mars has cyclic weather with surface temperatures ranging approximately from  $-120\text{ }^{\circ}\text{C}$  to  $-14\text{ }^{\circ}\text{C}$  and pressure from 6.8 hPa to 9 hPa. Despite seeing some chemical activity in the Martian soil, the Viking missions provided no evidence of life on Mars. [5.]

## 2.2 FMI's role in Mars research

The FMI has contributed scientific instruments for various deep space exploration missions. The 2008 Phoenix lander, notable for confirming the presence of water ice on Mars, included a pressure instrument provided by FMI. The lander measured atmospheric pressure cycles and phenomena. [6.]

NASA's Mars Science Laboratory rover, Curiosity, touched down on the Martian surface over four years ago to date and is still delivering scientific measurements. Contained in the Rover Environmental Monitoring station (REMS) sensor suite are pressure and humidity instruments from FMI. [7.] In the future, FMI will continue its Martian research activities. They are to deliver pressure and humidity instruments for European Space Agency (ESA)'s ExoMars mission, scheduled to fly as soon as 2020. The METEO science package on board the ExoMars rover will contain two FMI instruments, METEO-H and METEO-P, for humidity and pressure measurements respectively. [8.]

## 2.3 MetNet mission overview

The MetNet mission is a joint project between FMI, Lavochkin Association, Russian Space Research Institute IKI and Spanish Instituto Nacional de Técnica Aeroespacial (INTA). Work on the project started in 2001, led and funded by FMI. The mission proposes to establish a surface network of weather stations on Mars. Meteorological and climatological research would benefit from simultaneous measurements from multiple locations. These light weight landers could be dispersed in numbers on a single flight to Mars, providing a

large coverage of the planet's surface. [9.]

The primary objective of the MetNet mission is meteorological and climatological research. The major phenomena of interest are atmospheric circulation patterns with related to the global cycles of CO<sub>2</sub>, H<sub>2</sub>O and dust, which are also intertwined with each other. Regional and local phenomena, e.g. dust raising mechanisms and the study of dust devils are also of interest. Research into climatological cycles and the general evolution of Martian climate could also benefit from this network. [9.]

Finnish Meteorological institute continues to work on the Mars MetNet Precursor Mission. The precursor mission serves to demonstrate the vital Entry-Descent-Landing (EDL) systems as well as the overall feasibility of the mission concept. By the end of 2016, two complete EDL systems have been manufactured and tested. Once deployed, the precursor lander is designed to conduct meteorological observations and gather data up to one Martian year, or 687 Earth days. [9.]

The MetNet system consists of multiple elements. The Inflatable Breaking Unit (IBU) and the inflatable heat shield, shown in figure 2, are in charge of ensuring the lander reaches the surface intact. Underneath the heat shield lies the surface-penetrating forebody. The shield's semi-rigid design is intended to absorb the shocks and vibrations of the landing, and ultimately, burrowing inside the Martian surface. Housed within this payload container are the scientific sensors and the computer system that operates them. [9.]

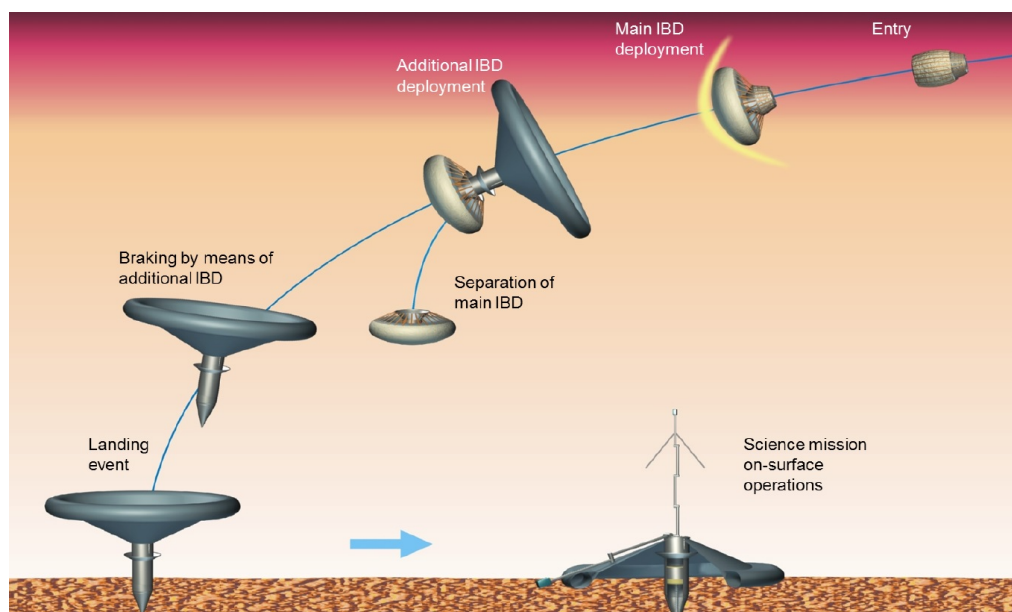


Figure 2: Landing concept. Copied from Harri et al. (2016) [9].

### 3 MetNet on-board computer

#### 3.1 General design information

The MetNet on-board computer is a light-weight custom-built PCB. The OBC is designed with reliability in mind to survive the difficult environment it is meant to operate in. It is built around two Freescale MC9S12XEP100 microcontrollers, and all the control and communications interfaces are duplicated for redundancy. [10.]

The OBC breadboard is a hexagonal multi-layered PCB with components placed on both sides of the board. The PCB is carefully designed with attachment holes placed so as to provide increased protection against shocks and vibration. It is built to closely mimic the shape and dimensions of the payload bay it is housed in. [10.]

It is explicitly important to minimize the chances of failure in an environment that is inaccessible after deployment. With this in mind, the OBC is designed to include two Microcontroller Units (MCUs). This parallel processor design is envisioned to provide increased fault tolerance by allowing the other MCU to take over operational responsibilities in case of errors. Either processor may reprogram or even permanently disable the other should the need arise. As show in figure 3, all the control interfaces and memories on the OBC are duplicated as well, and both MCUs have access to all interfaces through their own signal paths. [9.]

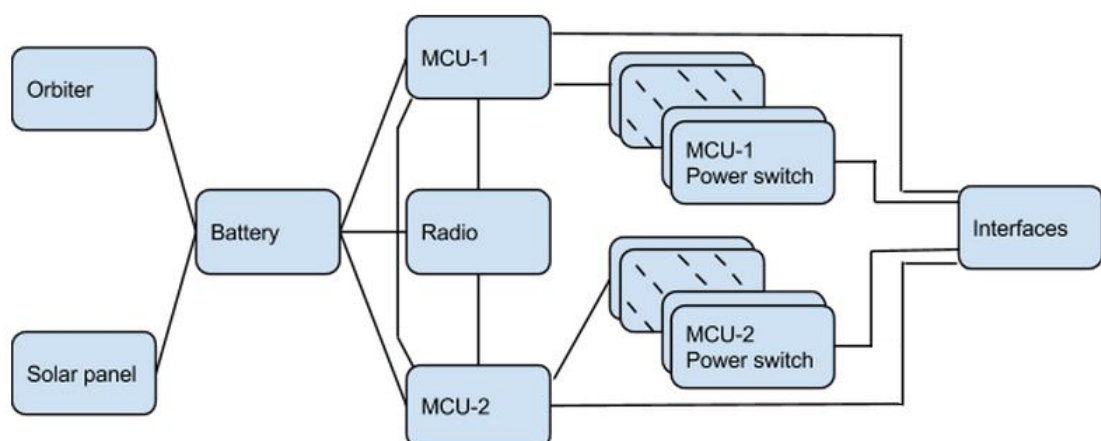


Figure 3: Block diagram. Copied from Rouhiainen (2015) [11].

The brains of the MetNet on-board computer are the two Freescale MC9S12XEP100 microcontrollers. The S12X is a commercial MCU, primarily used in automotive industry, and was not initially certified for space applications. The microcontrollers were successfully put through a space certification process by FMI.

The microcontroller underwent thermal qualification in the FMI space laboratory in Helsinki, Finland. Mechanical qualification of the MCU was conducted at HI-REL Laboratories, the USA. Furthermore, the plastic casing material of the chip was tested for outgassing by INTA. The microcontrollers passed all these tests. [12.]

In addition, ionizing radiation tests on the MCU were performed in 2015. The MCUs were dosed with Co-60 gamma radiation. These tests prove that the S12X MCU can withstand doses of radiation in excess of what is expected to be incurred on a trip to Mars. [13.]

### 3.2 Peripherals & interfaces

A number of sensors and peripherals will be connected to the OBC, as shown in the system structure below 4. The MNL sensor package responsible for atmospheric measurements consists of humidity, temperature and pressure sensors, as well as Solar Irradiance sensor and pyrometer. The panoramic camera will image the landing site and its surroundings. Most of the sensors will be connected to an RS422 compatible serial interface. As with the external flash memory chips, some of the sensors might be operated via Serial Peripheral Interface (SPI) as well. [10.]

As the lander will not be equipped with direct communications capability between the lander and Earth, a nearby spacecraft is required to act as a relay. The radio system implements the Proximity 1 protocol for compatibility with the established Mars platforms. [10.]

The power system provides 3.3 volts for the microcontrollers. The 5 and 12 volt lines serve the different sensors on board. [10.]

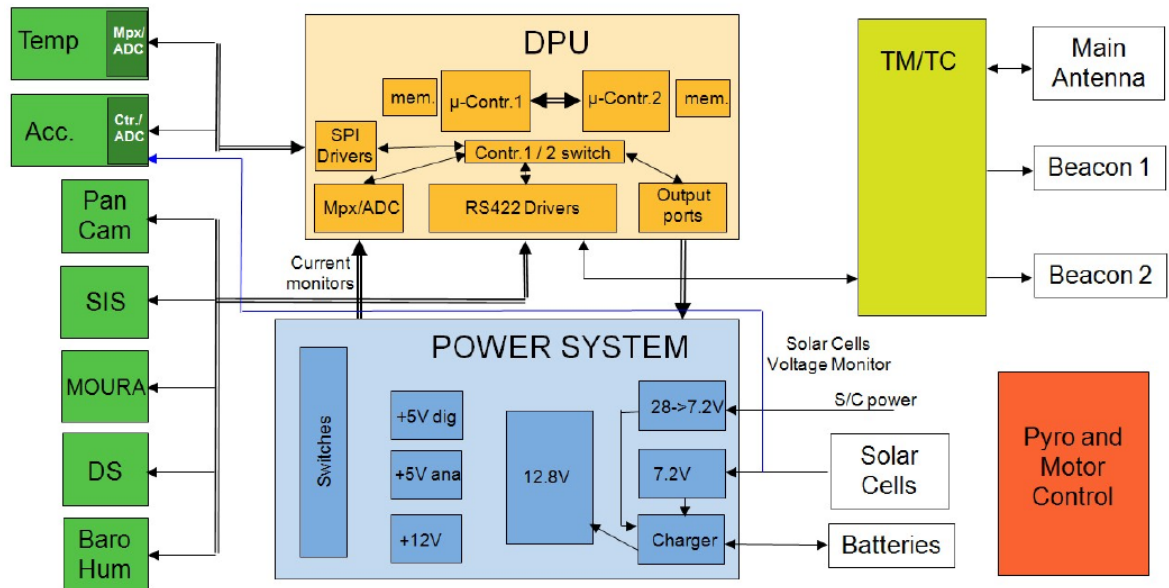


Figure 4: MNL system structure. Copied from Harri et al. (2016) [9].

### 3.3 Development process

It is worth noting that the development of hardware is an iterative process, in which each model will serve as a testbed for fixes and alternate designs. Several hardware revisions will be built during the MetNet project, the first prototype being the test model, built as a proof of concept for testing the systems design.

Identifying design issues in the earliest phases is critical, as introducing major architectural changes can become increasingly laborious the later in the project they occur. Consequently, the OBC hardware was altered from the Flight Model (FM) design to build the test model documented in this thesis. The modified shape and layout facilitate testing of key electronic circuits.

The FM design will be revised based on these findings and is intended to be implemented in all subsequent models. Furthermore, the completion of this TM milestone leads to an improved EM, built to correct dimensions.

## 4 Test environment and process

### 4.1 Test hardware and equipment

The OBC test model, figure 5, is a custom made PCB, designed to help testing. The environment the OBC was tested in consists of hardware and software components. The Freescale Codewarrior Integrated Development Environment (IDE) is the primary software development tool used in this project. Furthermore, the testing process required the use of several electronics laboratory tools, of which, some of the more important ones and their utility are described briefly in this section.

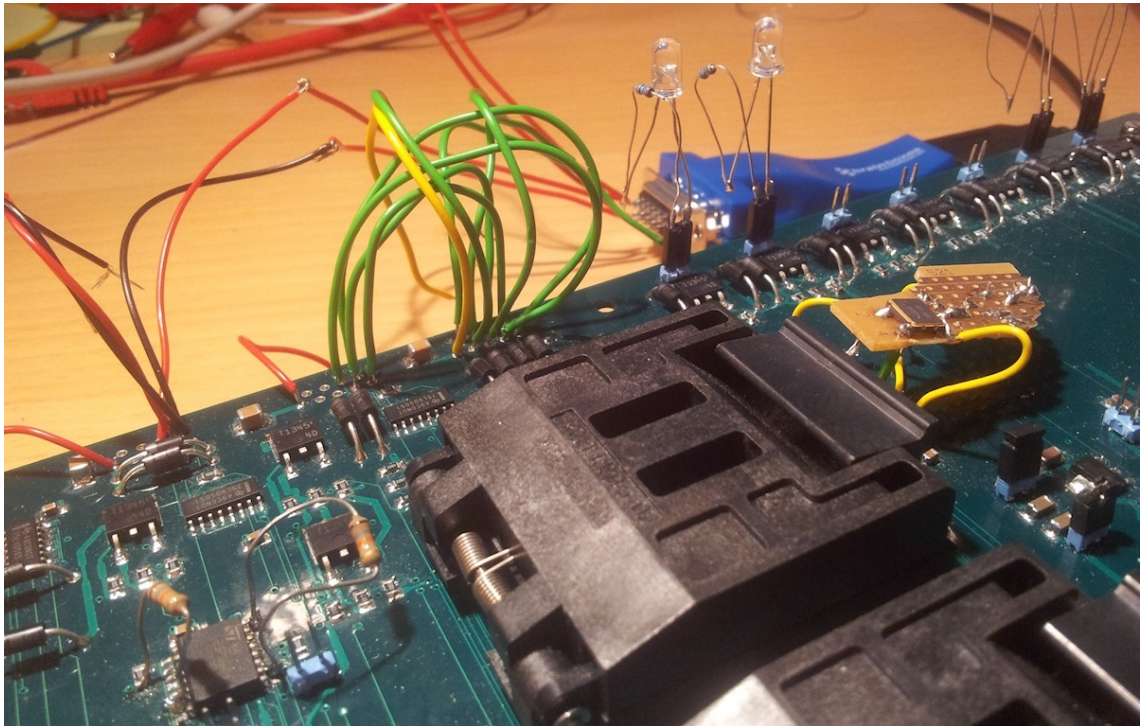


Figure 5: OBC with some modifications

The physical dimensions and the component layout of the TM had been altered from the upcoming design, to make testing of electronics easier. The board is rectangular instead of hexagonal, and the sensor interfaces are scattered on the outer edges with reasonable spacing around them. Many jumpers were included in the design to provide access and isolation to the power lines and their control interfaces. Instead of using space qualified components, the TM PCB was built with COTS parts.



An oscilloscope was needed to truly verify how serial communications interfaces behave, since it allows one to easily visualize multiple signals on the same time line. Indeed, inspecting detailed signal timing behavior is perhaps the key use for an oscilloscope, which makes it one of the most important debugging tools. Common adjustable settings include frequency and amplitude scales as well as being able to control the precise timing and capturing of a signal. A Tektronix TDS 360 oscilloscope was a huge help in debugging more than one problem.

The multimeter is one of the necessities of any electronics laboratory for its variety of useful debugging features. The primary purpose of the multimeter is measuring the three basic physical quantities - current consumption, voltage level and resistance. Additionally, some of the more advanced multimeters can aid in finding out whether signal paths are connected together, by emitting a sound when the probes are shorted. A Wavetek 15XL and a TENMA 72-6870 multimeter were used during testing of the OBC.

A TTI 1006 TGI function generator was used as an alternate clock source for the MCUs. The Power Supply Unit (PSU) used during testing was a TTI EL302RD.

Finally, being able to solder is a required skill for anyone working with electronics. Often it can be more efficient to hack something together rather than buy supplies, not to mention waiting through the ordeal of having PCBs built to order. Instead, it may be entirely possible to bypass a small oversight in the design with a wire and some components soldered together. During the testing discussed in this thesis, several prototype circuits and gadgets were created. Connectors, Light Emitting Diodes (LEDs), pull resistors, and other more complex circuits were utilized to fix problems on-the-go or aid with testing in other ways.



Figure 6: An LED with a 2 pin connector soldered in

## 4.2 Development of test software

Freescale's Codewarrior IDE was used for developing and debugging the software on the microcontrollers. The IDE is not radically dissimilar to other common software IDEs such as Visual Studio or Eclipse. It is not complicated to get started on a new project - all the commonplace tools and functions for creating and compiling projects are provided.

It could be argued, however, that the debugger, in figure 7, is vastly more important than the editor environment. The debugger lets the user step the program one instruction or line of code at a time, and importantly, the status of the processor and the contents of its memory are accessible to the user. In the debugger the highlighted lines denote the next instruction or line of code to be executed.

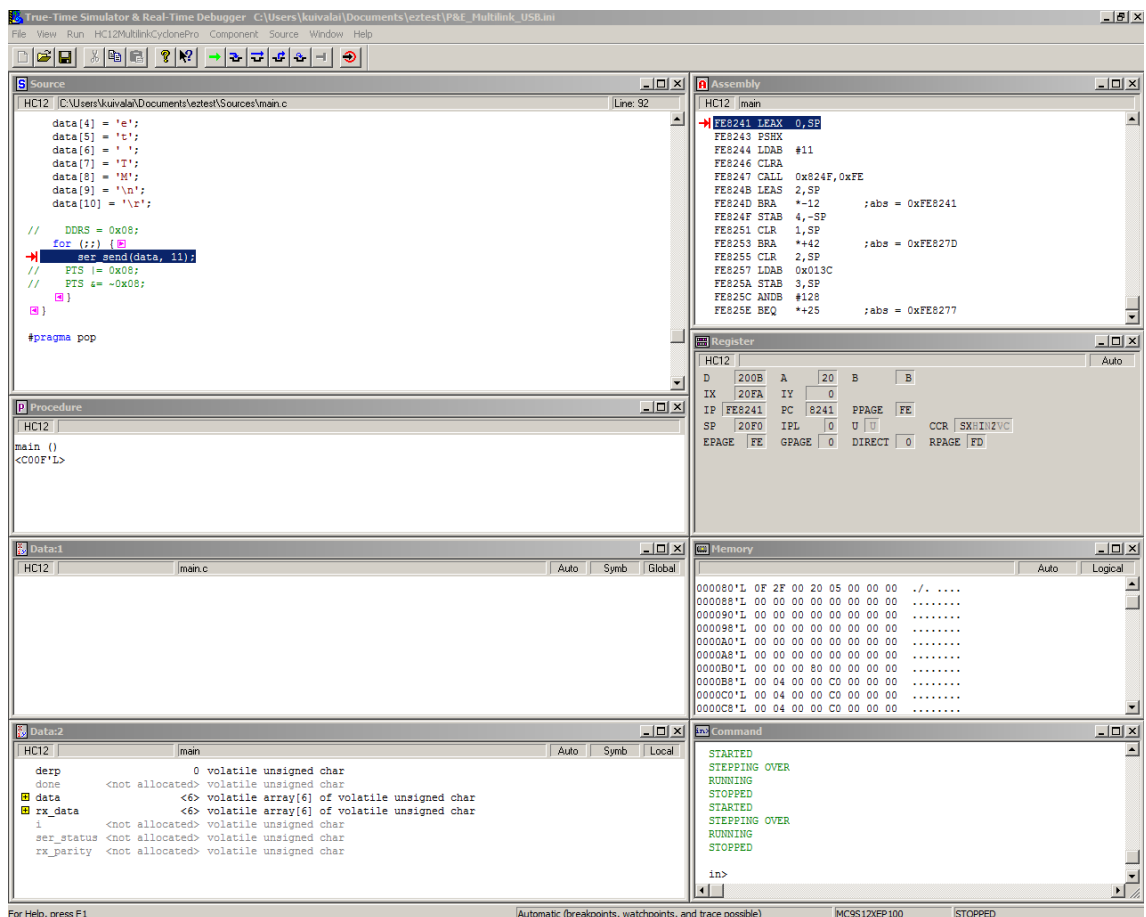


Figure 7: Screenshot of the debugger. [14]

A basic code base for the S12X MCU, consisting of a few modules, including io control and configuration, was provided by a colleague. The base code module organization is presented in table 1.

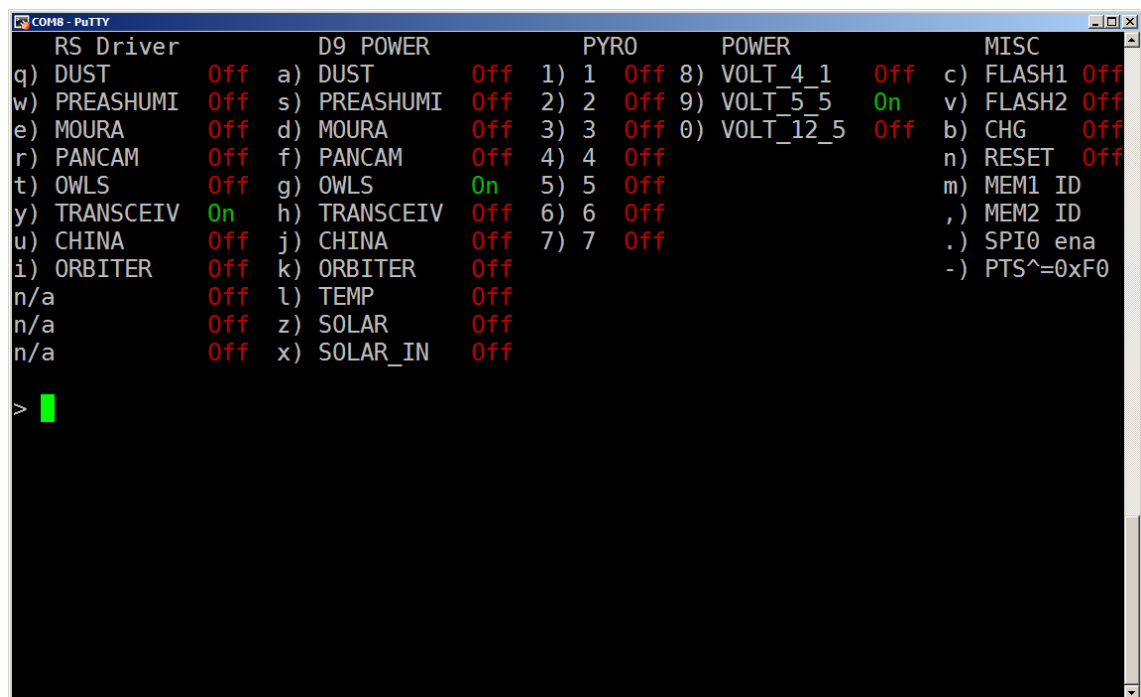


Table 1: The organization of the base source code modules

Module	Description
memory	Responsible for interfacing with the external flash memory.
io_ctrl	Contains functions for enabling power for pyros and instruments.
init_system	Handles the default boot state of GPIO pins and other system settings.
cpu_communication	Holds the CAN bus routines.
measure	Takes care of communicating with the instruments.
xgate	A co-processor within the S12X die. This module is meant to handle the external radio communications in the future.

Initially, several CodeWarrior projects were created to handle testing of different parts of the OBC. It was decided to first build each module into its own project file, from a blank slate, to avoid unnecessary complexity. For example, program code for operating the CAN and Serial Communications Interface (SCI) modules were first developed and tested on their own before being integrated into other project files.

Later, some of these test programs and prototypes were combined in order to create a more unified test application. This application, shown in figure 8, presents a terminal front-end that gives the user the ability to toggle any control interfaces via keyboard input, greatly easing the testing process.



```

COM8 - PuTTY
RS Driver      D9 POWER      PYRO          POWER          MISC
q) DUST        Off a) DUST        Off 1) 1  Off 8) VOLT_4_1  Off c) FLASH1 Off
w) PREASHUMI   Off s) PREASHUMI   Off 2) 2  Off 9) VOLT_5_5  On  v) FLASH2 Off
e) MOURA       Off d) MOURA       Off 3) 3  Off 0) VOLT_12_5 Off b) CHG    Off
r) PANCAM      Off f) PANCAM      Off 4) 4  Off          n) RESET  Off
t) OWLS        Off g) OWLS        On  5) 5  Off          m) MEM1 ID
y) TRANSCEIV  On  h) TRANSCEIV   Off 6) 6  Off          ,) MEM2 ID
u) CHINA       Off j) CHINA       Off 7) 7  Off          .) SPI0  ena
i) ORBITER     Off k) ORBITER    Off          -) PTS^=0xF0
n/a           Off l) TEMP        Off
n/a           Off z) SOLAR       Off
n/a           Off x) SOLAR_IN   Off
>

```

Figure 8: Screenshot of the terminal front-end for controlling the MCU interfaces.

## 5 Test plan and procedure

### 5.1 Reset switch

The interface responsible for resetting an MCU was tested according to the plan in table 2. The RESET pin is an active low pin which means that its function is activated by driving it to 0 volts. In the test model the RESET pin connects to a transistor switch that should pull the pin to 0 volts when activated by the other MCU. Both processors were programmed

Table 2: Test plan for the /RESET switch

Make sure that both MCUs are running.
Activate the reset switch from MCU-1.
Measure the voltage of the RESET-2 pin.
Deactivate the switch and observe whether MCU-2 reboots.

with identical software that lit up three LEDs sequentially when powered on. The passive MCUs software had a variable enabled that forced it to branch into an infinite loop leaving LED 3 on, while the active MCU waited for user input on the terminal interface.

When activated, however, the voltage of the RESET-2 pin was measured with a multimeter at 1.7 volts, which is above the RESET pin's low voltage threshold of 1.6 volts. At this point it was clear that the switch had to be altered, but the eventual modifications will not be presented in this thesis.

Still, to verify the reset functionality of the MCU, it was decided to disconnect the transistor switch circuit from the PCB, leaving the RESET-2 pin connected directly to the other controller. A pull-up resistor was added to the pin so as to not leave it vulnerable to a floating state. The test was again run, now successfully, as evidenced by the observation of the correct LED sequence. As expected, the voltage measured at the pin was 0 volts during activation.

## 5.2 Battery charging

After a successful launch, the OBC can get power from two sources. During transit, the orbiter vehicle will power the OBC with 28 volts through an 'umbilical cord'. This will come to an end when the lander is deployed to the surface, where its sole source of power generation are solar panels. That power has to be stored somehow, for the system to be able to operate during any time of day, and with freedom from the elements. With this in mind, the OBC is designed to operate in such fashion that all power is routed through a rechargeable battery. [9.]

There are two battery charging circuits on the PCB, one for the orbiter and the other for the panels. Both charger circuits were tested with an 8 volt Li-ion battery under varying conditions. In all tests a multimeter was connected between the battery and the OBC to measure the flow of current. Another multimeter was used to measure the voltage at various terminals. The test plan for the orbiter is listed in table 3.

Table 3: Test plan for the orbiter battery charging circuit

Connect 28 volts from the PSU to the POWER_FROM_ORBITER input on the OBC.
Connect the battery to the battery input on the OBC.
Power on the system,
Enable charging.
Measure the voltage and the current through the battery before and after.
Measure the voltage and the current of the power supply unit before and after.
Repeat measurements under different system loads and battery levels.

The orbiter charging circuit was tested in a room temperature setting with a laboratory PSU that provided 28 volts to the OBC. The charging current and voltage of the battery was measured under various system loads and battery levels. The results indicate that in the TM configuration, the orbiter charging interface provides up to 250 mA of current at around 8 volts. The efficiency of the orbiter charging circuit was then calculated to be around 70%.

The other charger circuit expects approximately 6 volts from the solar panels. First the solar panel charging circuit was tested in accordance to table 4 with a PSU voltage set to 6 volts, after which the performance of the charging circuit was tested under various loads. The CHG switch that controls the charging process was also tested successfully -

the microcontrollers were able to halt and resume charging at will.

Table 4: Test plan for the solar cell battery charging circuit

Connect 6 volts from the PSU to the SOLARCELL input on the OBC.
Connect the battery to the battery input on the OBC.
Power on the system.
Test if the CHG switch can control the charging by activating it.
Measure the voltage and the current through the battery before and after.
Measure the voltage and the current of the power supply unit before and after.
Repeat measurements under different system loads and battery levels.
Connect solar panels to the SOLARCELL input and repeat the tests.

Batteries have specific operating temperature ranges they should be charged or discharged in. The specifics vary between manufacturer and according to the chemical composition of the battery, but usually fall inside  $-20\text{ }^{\circ}\text{C}$  to  $60\text{ }^{\circ}\text{C}$  for lithium ion batteries. To comply with this requirement, the solar charger circuit was designed to automatically turn on a battery heater if the temperature is not within parameters. A Negative Temperature Coefficient (NTC) resistor (or thermistor), connected between ground and the appropriate pin on the charger chip, ensures that charging can happen only within the acceptable temperature range. The test plan is detailed in table 5.

Table 5: Test plan for the charger's temperature threshold function

Connect 6 volts from the PSU to the SOLARCELL input on the OBC.
Connect the battery to the battery input on the OBC.
Connect a potentiometer between the NTC input and ground.
Power on the system.
Activate charging.
Measure the voltage and the current through the battery before and after.
Adjust the resistance of the potentiometer down until charging stops.
Adjust the resistance up until charging begins again.
Measure the resistance.
Adjust the resistance further up until charging stops.
Measure the resistance.

The temperature threshold function of the LTC3652 charger chip was then tested with a 100k potentiometer connected to the NTC input. Battery charging was first enabled by activating the CHG switch. Varying the resistance demonstrated rough cut-off points at 27000 ohms and 5500, corresponding to  $0\text{ }^{\circ}\text{C}$  and  $40\text{ }^{\circ}\text{C}$  respectively.

Table 6: Test plan for the battery heater

Connect 6 volts from the PSU to the SOLARCELL input on the OBC.
Connect the battery to the battery input on the OBC.
Connect a resistor between HEATER output and ground.
Power on the system.
Activate charging.
Measure the voltage and the current through the battery before and after.
Measure the voltage and the current of the power supply unit before and after.
Measure the voltage and the current through the load resistor before and after.
Repeat measurements under different system loads.

After this the circuit responsible for controlling the heater was inspected<sup>6</sup>. A resistor was connected between the HEATER output and ground, through which the current and voltage was then measured with a multimeter. It was found that the heater was erroneously enabled at all times, even during charging. The design of the heater will be revised after the writing of this thesis.

Finally, the charger circuit was tested using actual solar panels. The testing was done during the summer of 2016 at the Finnish Meteorological Institute. A clear sunny afternoon provided an excellent opportunity to push the panels to their limits. Before connecting the panels to the OBC, their rough performance was measured by running current through several different resistors.

Then the panels were connected to the OBC and tested. This test also provided an opportunity to utilize the revised CAN circuit that was implemented around the same time. MCU-1 was programmed to command MCU-2 through the CAN bus to switch its internal running state, with each state having different number of identical LEDs enabled. Each LED increased the current consumption by 10 mA as measured with a multimeter at the battery's positive terminal. Current and voltage of the battery, and those from the solar panel were measured during each state. The efficiency of the charger circuit was then calculated to be at around 70%.

### 5.3 Sensor power interfaces

Multiple sensors will be connected to MetNet OBC. Most of them will draw power from 5 V interfaces, with a few having additional 12 volt lines. The sensor power circuits were tested according to the plan in table 7, by connecting a resistor between the power output pin and ground.

Table 7: Test plan for the sensor power interfaces

Connect the battery to the BATTERY+ input on the OBC.
Connect a resistor between the interface power output pin and ground.
Power on the system.
Measure the voltage and current through the load resistor before and after enabling power to the interface.
Measure the voltage and current of the power source during the aforementioned steps.
Do these tests with MCU-2 as well.
Take measurements from each power output pin of each interface.
Repeat measurements with other resistors, including 10 and 380 ohms.
Repeat the tests with orbiter battery charging enabled.
Repeat the tests with the solar cell battery charging enabled.

### 5.4 Pyrotechnics

The pyro or pyrotechnics circuits are meant to control what may eventually be incendiary devices or electric knives responsible for example jettisoning parachutes during landing. Voltage and current across each pyro interface was measured with several resistors according to the test plan in table 8. A Li-ion battery delivering slightly above 8 volts was used as a primary power source. A lab PSU was used in some measurements to charge the battery and provide additional power to the system.

Table 8: Test plan for the pyrotechnics interfaces

Connect the battery to the BATTERY+ input on the OBC.
Connect a resistor between the PYRO power output pin and ground.
Power on the system,
Measure the voltage and the current through the load resistor before and after enabling power to the interface.
Measure the voltage and current of the power source likewise.
Do these tests with MCU-2 as well.
Take measurements from all pyro interfaces.
Repeat measurements with other resistors, including 10 and 380 ohms.
Repeat the tests with orbiter battery charging enabled.
Repeat the tests with the solar cell battery charging enabled.

## 5.5 CAN bus

The MetNet lander uses the CAN bus for reliable messaging between the two microcontrollers. According to table 9, the CAN module was tested by sending short messages between MCUs via CAN0 bus. The receiving end was expected to flash an LED when the right message was received. The program was run but at first no messages were being received. It was soon found that the CAN bus requires a more complex circuit than

Table 9: Test plan for CAN bus

Power on the system.
Send a message from MCU-1 to MCU-2.
Observe whether the LED denoting a received message lights up.
Inspect the appropriate registers to confirm message was received.
Repeat the test with MCU-2 sending a message to MCU-1.

a regular crossover serial, where Transmit (TX) connects to Receive (RX) on the other end. Once the CAN bus was connected properly, the communications were again tested by trying to send a message from one MCU to the other. Now the other MCU confirmed the transmission by flashing LEDs on message reception. This was further verified with the debugger - inspecting the CAN module specific registers as well as the random access memory where the messages were stored showed that messages were now passing through.

## 5.6 RS422 interface

RS422 is a loosely defined protocol for differential signaling, which means that TX and RX each have two wires, positive and negative. The logic levels are decided by the voltage difference, rather than the absolute voltage, of these two wires. A '1' is generated if the voltage in the positive wire is higher than in the negative wire, and a '0' is produced when the opposite is true. [15.]

RS422 signaling is used in communicating with the various scientific sensors. All the RS422 line drivers on board the test model are connected to their dedicated software serial interface on MCU side. The drivers were tested 10 by establishing a link between the microcontrollers and a PC via a USB-RS422 dongle. On the PC side the PuTTY terminal application was used to talk to the MCU.

Table 10: Test plan for the RS422 interface

Connect the OBC to a PC with the USB RS422 adapter.
Open the adapter's COM port with a terminal client on the PC.
Power on the system using any suitable power source.
Observe whether the terminal menu is displayed.
Try to enter commands with the keyboard.

Unfortunately, the RS422 line drivers used in the test model were not able to interface with the provided Brainboxes USB RS422 adapter. Yet, while the SN75 chip is meant for low voltage applications, as its name hints, its pins are 5 volt tolerant. This gave some potential leeway, and it was found that a 5-volt MAX488 differential line driver could act as a relay between the SN75 Low-Voltage Differential Signaling (LVDS) chip and the RS422 adapter.



## 5.7 External memory

The external memory is an M25P16 flash memory chip that is operated via an SPI interface. Table 11 shows the test plan. According to the device's datasheet, the chip should respond to a 'Read Identification' command with the decimal string 32, 32, 21, 16. A successful reception of this sequence proves the SPI communications work, and that the flash memory is operational. The Read identification command was sent to the memory chip, alas nothing was received. It was decided to bring out the oscilloscope to visualize signal behaviour.

Table 11: Test plan for the external flash memory chips

Power on the system.
Use MCU-1 to read the identification string of the first memory chip.
Write, erase and read the same memory.
Repeat the same tests with the second memory chip.
Do these tests with MCU-2 as well.

Figure 9 shows the oscilloscope view of the read identification data transmission. First the master device initiates the SPI transmission by pulling slave select (R1) low. This selects the device and the chip becomes active. Then the read identification command is sent bit by bit. Label 2 is the master clock and label 1 is the read identification command (0x9F). The R2 signal is the data coming from the memory chip.

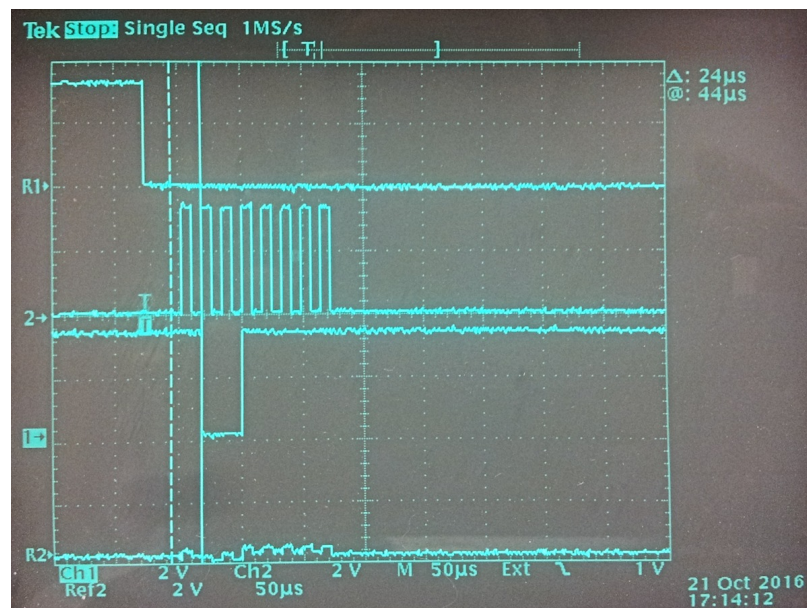


Figure 9: SPI transmission with invalid SPI settings.

At this point there was no reply from the chip. After careful inspection of the data and clock lines with an oscilloscope, it was found that the SPI clock phase setting was incorrectly configured. The clock phase setting determines on which edge the data is sampled at. The highlighted area in figure 9 shows that the clock signal transitions three times before the first falling edge of the control byte 10011111, indicating that the clock phase is wrong.

The SPI modes supported by the memory chip are either mode 0 (POL=0, PHASE=0) or mode 2 (POL=1, PHASE=1). The software was modified to use mode 0, which sets the output data to be sent at the falling edge, and the data capturing to occur at the rising edge. The correct SPI settings can be seen in figure 10. Of note is that there are only two clock transitions before the falling edge on signal 1.

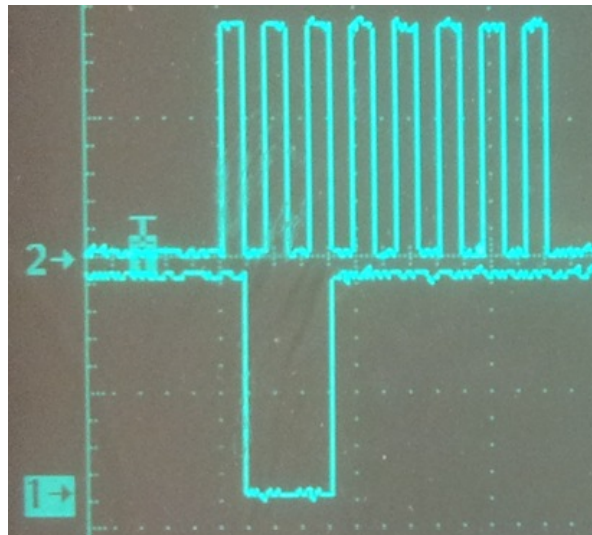


Figure 10: SPI transmission with correct SPI settings.

Once the correct settings were implemented the chip replied with the read identification sequence 32, 32, 21, 16, shown in figure 11. The highlighted 128 microsecond wide area contains 8 bits and spells the number 21.

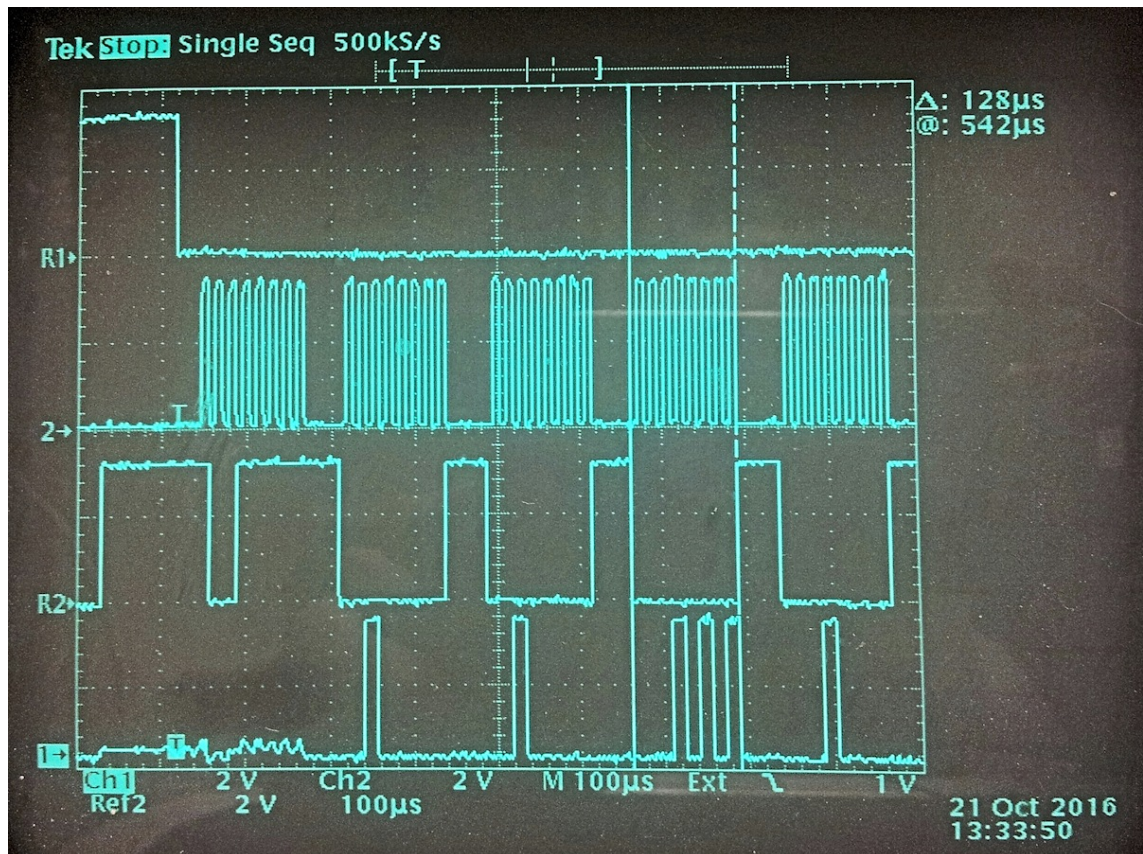


Figure 11: The read identification sequence.

The flash chips were then further tested - a program was written that performed reading, writing and erasing operations on the chips. Both MCUs were able to access both memory chips. This was confirmed by reading the processor's register values in the debugging environment and viewing the oscilloscope output.

## 6 Test results

A list of all the proposed changes to the design are listed in the appendix. 1 It contains not just the additions described in this section, but also changes proposed earlier in the testing process.

### 6.1 Reset switch

The reset switch did not behave as specified, because the voltage at the /RESET pin was 1.7 volts, which is slightly above the low voltage threshold of 1.6 volts. The reset switch will have to be modified so that when activated the voltage at the /RESET pin drops to as close to 0 volts as possible.

### 6.2 Battery charging

The temperature threshold function of the LTC3652 battery charger chip was tested to work. It was also found that the heater was not disabled while the battery charging was enabled. The switch will have to be revised.

Table 12 contains measurements using the orbiter to charge the battery. The results show the rough efficiency of the system.

Table 12: Battery charging measurements with 28 V to orbiter input

Battery voltage and current (CHG off)	PSU voltage and current (CHG off)	Battery (CHG on)	PSU (CHG on)	Battery charging current
8.14 V 0.06 A	28 V 4 mA	8.40 V -0.185 A	28 V 93 mA	0.24 A
7.61 V 0.06 A	28 V 4 mA	7.77 V -0.19 A	28 V 95 mA	0.25 A
7.57 V 0.09 A	28 V 4 mA	7.73 V -0.16 A	28 V 95 mA	0.25 A
8.07 V 0.04 A	28 V 4 mA	8.22 V -0.09 A	28 V 54 mA	0.13 A

Battery charging measurements using solar panels are listed in table 15. The results

show the efficiency of the system is approximately 70%.

Table 13: Battery charging measurements with 6 V to solar cell input

Battery voltage and current (CHG off)	PSU voltage and current (CHG off)	Battery (CHG on)	PSU (CHG on)	Battery charging current
8.07 V 0.04 A	6 V 0 A	8.21 V -0.1 A	6 V 0.3 A	0.14 A
8.08 V 0.04 A	6 V 0 A	8.20 V -0.07 A	6 V 0.255 A	0.11 A
8.08 V 0.04 A	6 V 0 A	8.21 V -0.08 A	6 V 0.271 A	0.12 A
8.09 V 0.04 A	6 V 0 A	8.22 V -0.12 A	6 V 0.324 A	0.16 A

The tested parameters of the panels are listed in table 14.

Table 14: Solar panel measurements with resistors

Resistance	Voltage	Current
9.97 k	8.10 V	0.78 mA
1.767 k	8.25 V	4.54 mA
382	8.12 V	20.3 mA
3	4.72 V	1300 mA

Table 15: Battery charging measurements with solar panels

Battery voltage and current (CHG off)	Battery (CHG on)	Panel (CHG on)	Battery charging current
7.66 V 33 mA	7.99 V -266 mA	7.49 V 437 mA	0.3 A
7.65 V 43 mA	7.99 V -256 mA	7.49 V 437 mA	0.3 A
7.64 V 52 mA	7.99 V -246 mA	7.49 V 437 mA	0.3 A
7.60 V 90 mA	7.94 V -207 mA	7.49 V 437 mA	0.3 A

### 6.3 Sensor power interfaces

The 5 V power interface results in table 16 indicate that the switches do not provide enough current.

The results in table 17 further confirm the findings of table 16.

Table 16: 5 V power interface measurements with 8.5 V PSU to BATTERY+ input

Load resistor	Load voltage and current (Power on)	PSU voltage and current (Power off)	PSU (Power on)
10 ohm	4 V 0.44 A	8.58 V 55 mA	8.58 V 0.5 A
47 ohm	5.05 V 103.5 mA	8.58 V 56 mA	8.58 V 160 mA

Table 17: 5 V power interface measurements with 28 V PSU to ORBITER input

Load resistor	Load voltage and current (Power on)	PSU voltage and current (Power off)	PSU voltage and current (Power on)	Battery (Power off)	Battery (Power on)
10 ohm	2.4 V 0.245 A	28 V 4 mA	28 V 4 mA	8.14 V 45 mA	7.94 V 0.30 A
10 ohm	3.25 V 0.37 A	28 V 52 mA	28 V 96 mA	8.23 V -0.08 A	8.02 V 0.18 A
47 ohm	4.93 V 91.2 mA	28 V 4 mA	28 V 4 mA	8.15 V 41 mA	8.06 V 132 mA
47 ohm	4.93 V 92.8 mA	28 V 37 mA	28 V 66 mA	8.2 V -39 mA	8.19 V -33 mA
380 ohm	5.14 V 13.42 mA	28 V 4 mA	28 V 4 mA	8.11 V 41 mA	8.1 V 55 mA
380 ohm	5.14 V 13.42 mA	28 V 36 mA	28 V 40 mA	8.11 V -38 mA	8.1 V -38 mA

It was found that the 12 V power interface switch did not heed the interface control signal. The circuit let current through the load resistor as long as the 12 V power was enabled. The switch design has been updated in the next version of the OBC. Measurements with various power sources are collected in tables 18, 19 and 20.

Table 18: 12 V power interface measurements with 8.5 V PSU to BATTERY+ input

Load resistor	Load voltage and current (Power on)	PSU voltage and current (Power off)	PSU (Power on)
10 ohm	3.3 V 0.33 A	8.58 V 55 mA	8.58 V 346 mA
47 ohm	11.8 V 0.18 A	8.58 V 55 mA	8.58 V 380 mA
380 ohm	12.14 V 31.8 mA	8.58 V 55 mA	8.58 V 113 mA

Table 19: 12 V power interface measurements with 28 V PSU to ORBITER input

Load resistor	Load voltage and current (Power on)	PSU voltage and current (Power off)	PSU voltage and current (Power on)	Battery (Power off)	Battery (Power on)
47 ohm	11.56 V 196 mA	28 V 4 mA	28 V 4 mA	8.08 V 45 mA	7.55 V 0.42 A
47 ohm	11.83 V 200 mA	28 V 47 mA	28 V 96 mA	8.24 V -0.06 A	7.82 V 0.16 A
57 ohm	11.53 V 169 mA	28 V 4 mA	28 V 4 mA	8.08 V 45 mA	7.78 V 0.36 A
57 ohm	11.52 V 172 mA	28 V 60 mA	28 V 97 mA	8.24 V -0.09 A	8.04 V 0.10 A

Table 20: 12 V power interface measurements with 6 V PSU to SOLARCELL input

Load resistor	Load voltage and current (Power on)	PSU voltage and current (Power off)	PSU voltage and current (Power on)	Battery (Power off)	Battery (Power on)
47 ohm	11.83 V 198 mA	6 V 324 mA	6 V 545 mA	8.22 V -0.12 A	8.05 V 0.12 A

#### 6.4 Pyrotechnics

The results listed below indicate that components have to be changed, because the voltage drops very dramatically. The pyro current should be approximately 1 A. Table 21 lists measurements conducted with a 28 volt power source and table 22 with a 6 volt power source.

Table 21: Pyro measurements with 28 V PSU to ORBITER input

Battery voltage and current (Pyro off)	PSU voltage and current (Pyro off)	Battery (Pyro on)	PSU (Pyro on)	Pyro voltage and current	Resistor
8.22 V -0.14 A	28 V 71 mA	8.04 V 0.12 A	28 V 96 mA	0.455 V 0.33 A	1 ohm
8.07 V 0.04 A	28 V 4 mA	7.86 V 0.25 A	28 V 4 mA	2 V 0.2 A	10 ohm
8.22 V -0.08 A	28 V 54 mA	8.02 V 0.1 A	28 V 97 mA	3.15 V 0.32 A	10 ohm
8.07 V 0.04 A	28 V 4 mA	7.98 V 0.11 A	28 V 4 mA	3.77 V 74 mA	47 ohm
8.22 V -0.09 A	28 V 54 mA	8.21 V -0.08 A	28 V 79 mA	3.78 V 75 mA	47 ohm

Table 22: Pyro measurements with 6 V PSU to solar cell input

Battery voltage and current (Pyro off)	PSU voltage and current (Pyro off)	Battery (Pyro on)	PSU (Pyro on)	Pyro voltage and current	Resistor
8.07 V 0.04 A	6 V 0 mA	7.88 V 0.27 A	6 V 0 mA	0.34 V 0.235 A	1 ohm
8.21 V -0.1 A	6 V 300 mA	8.02 V 0.13 A	6 V 548 mA	0.57 V 0.4 A	1 ohm
8.08 V 0.04 A	6 V 0 mA	7.92 V 0.25 A	6 V 0 mA	0.8 V 0.2 A	3.3 ohm
8.2 V -0.07 A	6 V 255 mA	8.04 V 0.12 A	6 V 548 mA	1.35 V 0.38 A	3.3 ohm
8.08 V 0.04 A	6 V 0 mA	8.01 V 0.11 A	6 V 0 mA	3.77 V 0.075 A	47 ohm
8.21 V -0.08 A	6 V 271 mA	8.21 V -0.08 A	6 V 397 mA	3.78 V 0.075 A	47 ohm



## 6.5 CAN bus

The CAN bus pins were initially connected wrong. A replacement circuit, figure 12, for a transceiverless CAN bus was found online.

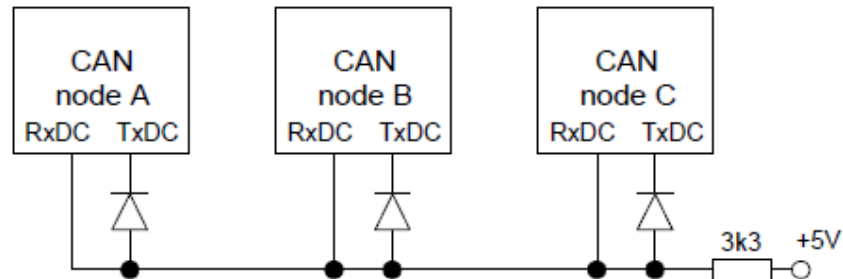


Figure 12: Connection of CAN nodes without CAN transceiver [16]

## 6.6 RS422 interface

The low-voltage RS422 line drivers used in the test model were not able to directly interface with the provided Brainboxes USB RS422 adapter. Still, the LVDS chip has 5-volt tolerant pins which allowed it to at least receive data from the adapter.

A 5-volt MAX488 differential line driver was first tested as a relay between the SN75 LVDS chip and the RS422 adapter. The differential TX line from the OBC's RS422 interface is connected to the differential RX line of the MAX488 chip, and the TX line of the MAX488 chip is in turn connected to the RX line of the USB adapter. Finally, the normal RX and TX pins of the MAX488 chip are short-circuited, which turns the line driver into a repeater. The relay approach worked and the terminal interface was successfully tested.

## 6.7 External memory

It was found that both Freescale MC9S12XEP100 processors could access both memory chips successfully. That being said, there is one potential problem with the way the circuit is currently connected. Because the pins are shared between the MCUs, the other MCU has to disable its SPI modules and switch the pins to high impedance inputs to allow the other MCU to access either memory. It is imperative that the same SPI bus is not



simultaneously used by both MCUs, as no operation can occur if for example slave select can not be pulled down to 0 volts because the other MCU is trying to drive it up to 3.3 volts.

Some changes were made to the circuit as suggested by the manufacturer. According to the chip's datasheet, the clock and slave select lines should never be pulled high at the same time. A pull-down for serial clock and a pull-up for slave select pins were introduced to satisfy this requirement. The pull-up resistor for the slave select pin is also meant to ensure the chip is not inadvertently selected, should the line become high impedance. These modifications are subject to change depending on the components chosen and the final composition of the OBC.

## 7 Conclusion

This thesis presents background for the MetNet mission, a brief description of the OBC, the test environment and details some test procedures and the results of these tests. The goal of this thesis was to test some of the circuits and interfaces of the OBC test model.

The process began by listing the testable circuits and then devising the test procedures for each circuit. Preliminary software was first built to operate the Freescale microcontrollers on the OBC, after which a more robust terminal interface for controlling the OBC's interfaces was built.

Issues were identified in some areas of the OBC as a result of these tests. Some circuits were amended while others may have required a complete redesign. For example, the CAN bus circuit was connected in a wrong way and required additional components and altered logic in connecting the signals.

With the results from these tests the, work continues on improving the OBC towards flight model. The test environment can still be improved by adding the ability to control the other MCU simultaneously from the terminal interface.

## References

- 1 Charles Q. Choi. Mars facts: Life, water and robots on the red planet website. [online].  
URL: <http://www.space.com/47-mars-the-red-planet-fourth-planet-from-the-sun.html>.  
Accessed 23rd November 2016.
- 2 National Aeronautics and Space Administration. Mariner 4. [online].  
URL: <http://nssdc.gsfc.nasa.gov/nmc/spacecraftDisplay.do?id=1964-077A>.  
Accessed 13th December 2016.
- 3 Perminov V.G. The difficult road to Mars: A brief history of Mars exploration in the Soviet Union. [online].  
URL: <http://history.nasa.gov/monograph15.pdf>.  
Accessed 15th November 2016.
- 4 Space Research Institute of the Russian Academy of Sciences. Mars 3 orbiter. [online].  
URL: <http://www.iki.rssi.ru/eng/pe.html/>.
- 5 National Aeronautics and Space Administration. Viking mission to Mars document. [online].  
URL: [http://www.jpl.nasa.gov/news/fact\\_sheets/viking.pdf](http://www.jpl.nasa.gov/news/fact_sheets/viking.pdf).  
Accessed 17th November 2016.
- 6 Ilmatieteen laitos. Phoenix-luotain vie Ilmatieteen laitoksen painemittalaitteen Marsiin website. [online].  
URL: <http://ilmatieteenlaitos.fi/tiedote/1185859119>.  
Accessed 2nd September 2016.
- 7 Ilmatieteen laitos. MSL-laskeutuja vie Ilmatieteen laitoksen tutkimuslaitteita Marsiin website. [online].  
URL: <http://ilmatieteenlaitos.fi/tiedote/445085>.  
Accessed 5th September 2016.
- 8 European space Agency. Robotic exploration of Mars: ExoMars 2020 surface platform website. [online].  
URL: <http://exploration.esa.int/mars/56933-exomars-2020-surface-platform/>.  
Accessed 5th December 2016.
- 9 Harri, A.-M. and Pichkadze, K. and Zeleny, L. and Vazquez, L. and Schmidt, W. and Alexashkin, S. and Korablev, O. and Guerrero, H. and Heilimo, J. and Uspensky, M. and Finchenko, V. and Linkin, V. and Arruego, I. and Genzer, M. and Lipatov, A. and Polkko, J. and Paton, M. and Savijärvi, H. and Haukka, H. and Siili, T. and Khovanskov, V. and Ostesko, B. and Poroshin, A. and Michelena-Diaz, M. and Siikonen, T. and Palin, M. and Vorontsov, V. and Polyakov, A. and Valero, F. and Kemppinen, O. and Leinonen, J. and Romero, P. The MetNet vehicle: A lander to deploy environmental stations for local and

- global investigations of Mars. Geoscientific Instrumentation, Methods and Data Systems Discussions. 2016;2016:1–32.  
URL: <http://www.geosci-instrum-method-data-syst-discuss.net/gi-2016-19/>>.
- 10 Finnish Meteorological Institute. MetNet experiment interface document. Accessed 11th September 2016. Available: FMI-MMPM-EID-01-Rev\_1\_6.pdf.
- 11 Rouhiainen, Taavi. Electronics of the on-board computer for Mars meteorological network stations; Marsin meteorologisen verkkoaseman ohjaustietokoneen elektroniikka. G2 Pro gradu, diplomityö. 2015-06-10.  
URL: <http://urn.fi/URN:NBN:fi:aalto-201506303500>>.
- 12 Nikkanen, Timo. Kontrolleri paine- ja kosteusinstrumentille Marsin kaasukehään; Controller for a pressure and humidity instrument in Martian atmosphere. G2 Pro gradu, diplomityö. 2014-02-10.  
URL: <http://urn.fi/URN:NBN:fi:aalto-201402181416>>.
- 13 Tapani Nikkanen, T. and Hieta, M. and Schmidt, W. and Genzer, M. and Haukka, H. and Harri, A.-M. Ionizing radiation test results for an automotive microcontroller on board the Schiaparelli Mars lander. In: EGU General Assembly Conference Abstracts. vol. 18 of EGU General Assembly Conference Abstracts. 2016. p. 16140.
- 14 True-Time Simulator & Real-Time Debugger [computer program]. NXP, Eindhoven, Netherlands
- 15 Hein Marais. RS-485/RS-422 circuit implementation guide. [online]. URL: <http://www.analog.com/media/en/technical-documentation/application-notes/AN-960.pdf>. Accessed 25th May 2016.
- 16 Jens Barrenscheen. On-board communication via CAN without transceiver. [online]. URL: [http://www.mikrocontroller.net/attachment/28831/siemens\\_AP2921.pdf](http://www.mikrocontroller.net/attachment/28831/siemens_AP2921.pdf). Accessed 3rd October 2016.

## 1 List of proposed changes

### 1.1 PCB schematic

Remove X9 connector

Swap source and drain of TR74 (solar charging transistor for LTC4412)

Remove diodes D1 and D2

LT3652 (U33) SHDN must be connected to V\_in and remove R171-174

Outputs (EXTAL) of both oscillators must be fixed from 3v3 to 1v8

LTC3112 (U41) RUN pin should be connected to solar cell input

Remove R34, R39.

Connect U37 SHDN to V\_in

Combine VDD1 & VDD2 into VDD

Combine GND & GND1 into GND

Charge output value for U41 from 9.12 to 11.7 v

Remove R185, R204

Change all diodes to SMD diodes, 1N5819 and 1N5822 to MBRS340T3G

Remove R43 & R44 to enable MCU1 debugging.

Remove R149 & R150 to enable MCU2 debugging.

Add pull up resistor to FLASH1 & FLASH2

Add pull down resistor to SCK1 & SCK3

Connect both MCU's CAN0 pins together, add diodes to TX pins and a pull-up to the circuit

Connect both MCU's CAN1 pins together, add diodes to TX pins and a pull-up to the circuit

Fix footprints for following components:

Bottom layer: C1, C5, C7, C11, C3, C9, C70, C74, C66, C72, C64, C88, L2

Top layer: L1, L3, L4, L5, C107, C109, C111, C113, R208

Fix values for following components:

Bottom layer: C13, C14, C15, C76, C77, C78 to 220 nF; C81 to 100 nF

Top layer: R187, R188, R206, R207; C80 to 100 nF

## 1.2 PCB layout

Swap component to other side:

Bottom layer: D109, D133, D14

Make space around interfaces

Turn Pyro4 output 180 deg

Change Pyro GND into THICK signal and combine into ground near battery